Available online at www.sciencedirect.com
ScienceDirect
Physics Procedia 1 (2008) 565–572
Physics Procedia
www.elsevier.com/locate/procedia

Proceedings of the Seventh International Conference on Charged Particle Optics

3D microscopic model of electron amplification in microchannel amplifiers for maskless lithography

Anton S. Tremsin[a]*, Harry F. Lockwood[a], David R. Beaulieu[a], Neal T. Sullivan[a], Eric Munro[b], John Rouse[b]

[a]*Arradiance, Inc., 142 North Road,Suite F-150, Sudbury MA 01776, U.S.A.*
[b]*Munros Electron Beam Software Ltd, 14 Cornwall Gardens, Londo, SW7 4AN, England*

Received 9 July 2008; received in revised form 9 July 2008; accepted 9 July 2008

Abstract

A novel approach for high-throughput maskless lithography is being developed by Arradiance Inc. The patented core technology is based on the combination of field emitters and microchannel electron amplifiers (MCAs) to produce a large array of individually controlled, high brightness electron beams. Brightness, stability, beam to beam uniformity, energy spread, achievable current, and many other parameters must be optimized simultaneously over a large field. Many of these parameters are determined by the characteristics of the amplification process in the MCA array that amplifies, stabilizes and shapes each electron beam. This paper describes a new three dimensional Monte Carlo model of the electron amplification process in a single microchannel. For a given input current and known MCA parameters, we calculate the (generally nonlinear) potential distribution along the channel utilizing a macroscopic saturation model. The static (3D with axial symmetry) electric field is calculated in and around the microchannel from the predicted potential distribution. That field is used to calculate individual electron trajectories along the pore length until their subsequent collision with the pore walls or arrival at the pore exit. The amplification process caused by secondary electron emission from those collisions is modelled for each electron. Evaluation of a large number of input electrons allows the MCA output to be predicted. The model is very useful for optimization of the MCA structure and operational parameters to meet the requirements of high-throughput lithography.

PACS: 85.40.Hp; 02.70.Uu; 07.77.Ka; 79.70.+q

Keywords: Maskless lithography; Microchannel amplifier; Monte Carlo model; Source optimization

1. Introduction

A number of novel techniques are being developed for high-throughput maskless lithography. Among them are a few utilizing direct writing by electron beams. Although features as small as 10 nm can be written by a single electron beam the throughput of a single beam system impedes its application in lithography. Application of multiple electron beams in parallel is one of the obvious ways to increase the throughput. The approach developed

* Corresponding author. Tel.: +1-978-369-8292; fax: +1-978-369-8239
E-mail address: atremsin@arradiance.com

doi:10.1016/j.phpro.2008.07.139

by Arradiance is based on combination of field emitters and microchannel electron amplifiers (MCAs), producing a large number of individually controlled high brightness electron beams [1]. All the components of the developed source are solid state and all the beams are defined simultaneously with lithographic accuracy. In order to meet throughput and lithographic requirements the source brightness, stability, beam-to-beam uniformity, energy spread, achievable current, and many other parameters must be optimized simultaneously over a large field. Many of these parameters are determined by the characteristics of the amplification process in the MCA array that amplifies, stabilizes and shapes each electron beam.

The model presented in this paper allows one to predict the MCA output characteristics and thus to optimize the MCA parameters in order to achieve the best source performance. In addition to energy and angular distribution of output electrons the model allows for calculation of timing characteristics of electron multiplication within an MCA pore.

2. Microscopic Monte Carlo model of MCA operation

The operation of MCA is very similar in principle to the operation of microchannel plates widely used in many applications requiring electron amplification, such as photon and charged particle detection, image intensifiers, and many others. Despite their wide use the output distribution from an MCP pore was not thoroughly studied and there is only limited data available now. Previous experimental investigations on the output energy and angular distributions [2]-[4] have sometimes contradictory results. Analytical attempts to predict the pore output did not yield detailed information due to a very limited statistics from Monte Carlo simulations [5] or only predicted the total output current without information about angular and energy distributions [6][7]. A very good summary of previously published work can be found in reference [5]. However it is the differential output distributions which are required for the brightness optimization of presently developed electron source for maskless lithography. The structure of the MCA can also be substantially varied compared to standard microchannel plate devices due to the fact that the MCA is engineered through lithographically determined patterns and can use completely different materials for current conducting and electron emission layers. Moreover, the signal amplification in the MCA does not require high gain operation but rather high stability and brightness. The latter fact leads to less stringent requirements on gain but at the same time demands better optimization of the output distribution. An experimental evaluation of the MCA output is obviously an inevitable requirement for the source characterization. However, an analytical model correlated with experimental data can be a very helpful tool for the source optimization, especially for those device parameters which require expensive and time consuming device modifications.

The statistical nature of signal amplification in the MCA pore makes it very difficult, if not impossible, to derive an analytical solution to the differential output distributions. Previous Monte Carlo models were also limited to a 2-dimensional geometry and the number of modelled single-electron amplification events was limited to only ~20 due to high demands on the computation time for each event.

The model described in the present paper is fully 3 dimensional although we limit calculations so far to the cases with axial symmetry (MCA pore does not have an angular tilt). The output distributions calculated with the help of our model and presented in Section 3 typically represent 100000 modelled electron amplification events.

We were able to substantially decrease the computational time and therefore to increase the model statistics due to several factors (not to mention the increase of computational power afforded by modern processors). First, for a given set of MCA parameters, the stationary electric field is calculated only once with software developed by MEBS [8] . Second, the numerical solution of electron motion equations is optimized with self adjusted length-of-time steps. The model does not use a fixed time interval for each iteration but rather adjusts the travelled distance, which is set not to exceed a given value.

2.1. Model parameters

- Vs- accelerating voltage applied across the pore,
- R - resistance of the pore,
- MCA potential distribution and the electric field inside the pore and in the vicinity of its output;
- MCA geometry (pore length, diameter, electrode penetration);
- electron emission properties of the pore surface (number of secondary electrons as a function of primary electron energy and angle, secondary electron energy and angular distributions).

2.2. Electric field inside the MCA pore

The precise description of an avalanche development inside an MCA pore is a very challenging problem due to required computational resources. The electric field inside the pore, strictly speaking, is a self-consistent field determined by: the accelerating electric field from bias Vs, the field of the wall charge (changing in time by the replacement current) generated by the previous electron collisions with the walls and by all the avalanche electrons inside the pore. In addition, a large number of electrons have to be tracked as the electron avalanche propagates along the pore. Self-consistency of the electric field requires recalculation of the field after each time step. Finally, any reasonable model prediction requires a large number of electron avalanche processes to be modelled. The computational time of full-scale Monte Carlo model, without any simplifications, would be extremely long even for a limited number of modelled events. However, some approximations (summarized below) can be used in the model and still lead to a reasonable agreement with the experimental data.

The first simplification used in the present model is related to the fact that the MCA will operate in a current amplifying/stabilizing mode after reaching a steady state. We do not intent to predict the dynamics of MCA stabilization. What we are optimizing with the help of this model is the MCA output signal assuming that it has already reached a steady state. Therefore we can use the macroscopic model of pore operation, which allows us to predict the potential distribution along the pore established in a steady state mode for a given set of MCA parameters. These macroscopic potential simulations are based on the previously published models developed for microchannel plates [6],[7]. The saturation model has only two free parameters to be extracted from experimental measurements: macroscopic gain coefficient (amplification per unit length of the pore at a given voltage) and MCA bias at unity gain. The results of the saturation model were proven to be in very good agreement with experimentally measured data for both microchannel plates and MCAs [1],[6],[7]. In saturation the potential distribution along the pore becomes very non-linear with most of the potential dropping along the initial section and thus corresponding to a reduced electric field in the output section. The field in the output section of the pore is reduced to the values corresponding to unity gain, i.e. each collision with the wall on average produces only one secondary electron. It is that saturation which leads to current stabilization in our electron source despite considerable fluctuations of the initial current generated by cold-cathode, field emitting arrays.

Fig. 1 shows the predicted potential distributions calculated for different levels of pore saturation caused by the increased input current (with MCA bias fixed at the same value). The corresponding calculated electron current inside the MCA pore Is (“signal current”) is shown in Fig. 2 as a function of distance along the pore. With no saturation the signal current Is increases exponentially, while in saturation it reaches a certain peak value some distance from the pore exit remaining constant for the rest of the pore. In the later case only the input section of the pore amplifies the signal, while the rest of the pore operates in “unity gain” mode. The level of saturation is determined by the three parameters: pore resistance, MCA bias and the input current. A proper pore resistance can be selected for a certain level of saturation at given input and output currents.

The potential distributions shown in Fig. 1 were used for calculation of the electric field inside the pore. The penetration of the metal electrode into the pore (“end-spoiling”) is taken into account in the field calculations, leading to varying field configurations obtained with different end-spoiling, Fig. 3. The field at the pore exit is very important for the output electron distributions as will be shown in Section 3 and is one of the parameters which can be optimized in order to reach the highest source brightness.

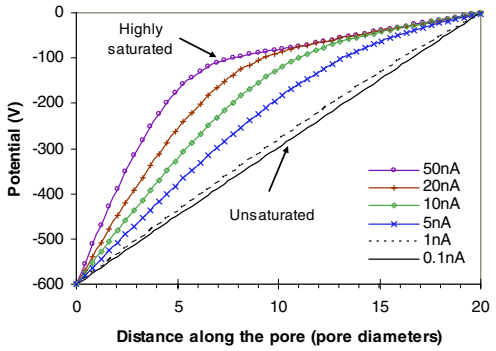

Fig.1. Potential distribution along the pore calculated with the help of macroscopic model. Saturation increases with the increase of input current (shown in the legend).

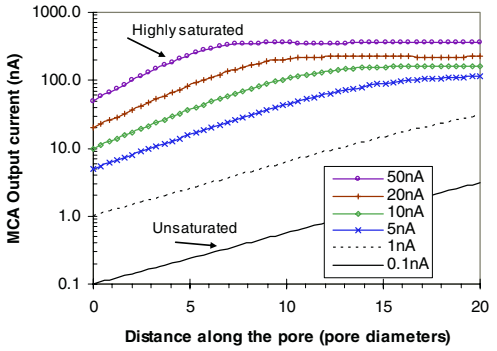

Fig. 2. The amplification of electron current along the pore calculated with macroscopic model. At saturation (corresponding to large input current) the output section of the pore operates in unity gain mode.

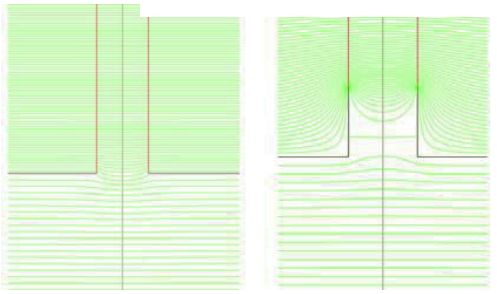

Fig. 3. Equipotential lines at the pore output. (left) no electrode penetration into the pore. (right) electrode penetrates by one channel diameter.

2.3. Model assumptions

Assumption 1: the electric field of avalanche electrons is disregarded as these electrons produce an electric field much smaller than the electric field from the external bias applied to the MCA and the field of the positive wall charge. The latter statement is obviously true for the case when electron density inside the avalanche is very small. The MCA pore typically will have an input current of I_o=1–10 nA. If electrons are uniformly distributed in time (the fluctuations of input current are relatively small) then the average interval between electrons arriving at the MCA input is: (q_e/I_o) ~ 10-100 picoseconds, comparable to the expected average electron transit time, well known from the previous MCP studies and confirmed by our model. The signal propagation inside the MCP pore takes place within several hundred picoseconds [9]. Thus, it can be assumed that there will be <10 incoming electrons for each "individual" electron multiplication process. The maximum gain of the MCA will not exceed a factor of 100, corresponding to the maximum output current of 0.1-1 μA. Within the virtual electron avalanche there will be $<10^3$ electrons, spread along the length of the pore. Assume that these 10^3 electrons are concentrated within a sphere with diameter equal to a smallest pore size (~2 μm).. The average distance between the electrons, in this extreme case, will be ~$[4/3\pi(2\ \mu m)^3/1000]^{1/3}$ ~0.3 μm resulting in an electric field: $E=1/(4\pi\varepsilon_0)q_e/d^2$ ~17 V/mm. The accelerating electric field from the potential Vs across the MCA is typically 1000 V/mm, about two orders of magnitude larger than the worst case scenario for the electron repulsion field. Therefore, the electric field component generated by the signal electrons will be disregarded in the initial Monte Carlo model.

Assumption 2: Taking into account assumption 1, the model introduces a 'test' electron that will represent the electron avalanche and will be followed as it propagates along the MCA pore. The concept of a 'test electron' was used in several previous modelling attempts [5],[10] and exhibited reasonable agreement with the experimental data. The electric field within the pore is assumed to reach a steady state when the pore saturation remains constant and the resulting non-linear electric field within the pore does not change during ~100 ps of electron propagation within the MCA pore.

2.4. Model flow

1. Static electric field is assumed to have been established in the pore. Potential distribution is calculated with the help of the macroscopic model.
2. Saturated 3-dimensional electric field (with axial symmetry) within the MCA pore is calculated for a given potential distribution.
3. Microscopic 3-dimensional Monte Carlo model calculates charge amplification for each incoming electron. A "test" electron is tracked along the pore, exciting secondary electrons upon collisions with the pore wall. Output distributions calculated from a large number of simulated electrons.

2.5. Signal amplification inside the MCA pore

Calculation of avalanche starts with the first secondary electron produced at the point where an input electron collided with the pore wall. The energy and collision angle of the input electron are generated according to distributions characteristic of a specific FEA source. On i^{th} time step the test electron represents a cloud of $N_s(i)$ signal electrons. When an electron from that cloud strikes the pore wall it excites $\delta(E_{in},\theta)$ secondary electrons into the pore. The number of secondary electrons depends on the collision energy E_{in} and angle of incidence θ and can be calculated from the following equations (according to refs. [11]-[13]):

$$\delta(E_{in},\theta=\frac{\pi}{2}) = P_s(0)\frac{E_{in}L_s}{\varepsilon R_p}\left(1-\exp(-\frac{R_p}{L_s})\right) \tag{1}$$

$$\delta(E_{in},\theta) = \delta(E_{in},\theta=\frac{\pi}{2})\exp\left[P(E_{in})(1-\sin\theta)\right] \tag{2}$$

where R_p = range of primary electrons in the glass, L_s = secondary electron escape length, $P_s(0)$ = surface escape probability, ε = energy required to create a single secondary electron.

Coefficient values used are the same as previously reported values for SiO_2 and electrode metal [5]:

	SiO_2	Nichrome
L_s	33 A	20 A
$P_s(0)$	0.15	0.024
ε	10 eV	6.65 eV

$$P(E_{in}) = 0.7664 - 1.533\exp\left[-3.598E_{in}\right], \tag{3}$$

where E_{in} is in keV.

The range of electrons R_p can be calculated from expression (according to Young [14])

$$R_p = 1.15e^{-4}(E_{in}[keV])^{1.35}/\rho[kg\cdot m^{-3}] \tag{4}$$

where ρ [kg m^{-3}] is density of material.

Hence, after the collision a new test electron represents $N_s(i+1) = N_s(i)\,\delta(E_{in},\theta)$ electrons. Each emitted electron has the energy E_{out} generated by a random number generator according to the distribution taken from the experimental results of Petrova et al. [15]

$$f(E_{out}) = C\left(\frac{E_{out}}{\langle E_{out}\rangle}\right)^{\beta}\exp\left[-\frac{\gamma E_{out}}{\langle E_{out}\rangle}\right] \tag{5}$$

where C is normalization constant, and parameters β and γ are 0.7 and 7, respectively, for SiO_2. The electron emission angle is usually assumed to have a cosine distribution = $\cos(\theta_{out})$, where θ_{out} is the angle relative to the normal to the surface. That distribution is independent of azimuth angle. However, some experiments indicate that the distribution deviates from an azimuth independent cosine for grazing incidence primary electrons, although such dependence is not well characterized at the present time.

After the emission from the pore wall the trajectory of test electron is calculated until its subsequent collision with the wall or ultimate emission from the MCA. When a 'test' electron exits the pore it represents the calculated N_s number of output electrons (the gain) and has a specific output energy and output angle. The modelling of amplification of a single electron avalanche does not reveal the characteristics of MCA operation. Therefore modelling of single avalanche propagation should be repeated a large number of times, producing a large number of 'test' electrons at the MCA pore output thus generating the output distributions that can be derived from these modelled single electron avalanche events.

3. Application of the model

The microscopic model can be very helpful in optimizing the source brightness and stability by predicting the performance of a particular MCA, substantially extending the very limited number of MCA configurations available for experimental evaluations. The model can estimate the ways to increase the brightness by modifying the pore geometry (length, diameter, electrode penetration, pore angular tilt, extraction field configuration), MCA level of saturation (pore resistance, accelerating bias, input current), multistage MCA operation, and etc. Even with a limited experimental correlation the model can predict the trends for the performance optimization if not exact values.

The results presented in this section illustrate the model capabilities for the source optimization. Improvement of source brightness is shown in the examples of pore saturation and electrode penetration. The graphs below intend to illustrate the effect of those parameters rather than to predict the source ultimate performance with respect to achievable brightness.

Figs. 4 and 5 show the integral output distributions calculated for an MCA operating at different levels of pore saturation. The output angular distribution becomes quite narrower for the saturation mode of amplification and peaks below 2 degrees. At the same time the percentage of low energy electrons is substantially increased at saturation. Therefore operating MCA in a saturated mode not only improves the source temporal stability but also increases its brightness.

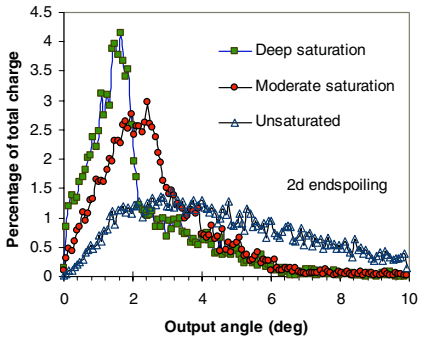

Fig. 4. Output angular distributions calculated at different levels of pore saturation. V_{MCA}=600V, L/D=20:1, R_{MCA}=500kΩ, Unity gain at `183V, Deep saturation corresponds to 50 nA input current, saturation = 10 nA and unsaturated = 0.1 nA input current.

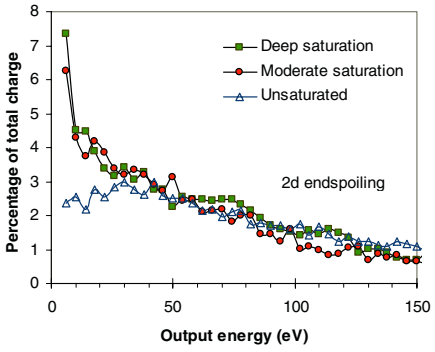

Fig. 5. Output energy distributions calculated at different levels of pore saturation. Parameters the same as in Fig.4.

Predicted differential output distributions (output energy distributions calculated for a given range of output angles) are shown in Fig. 6. These graphs show in more detail the variation of MCA output with the increase of saturation level.

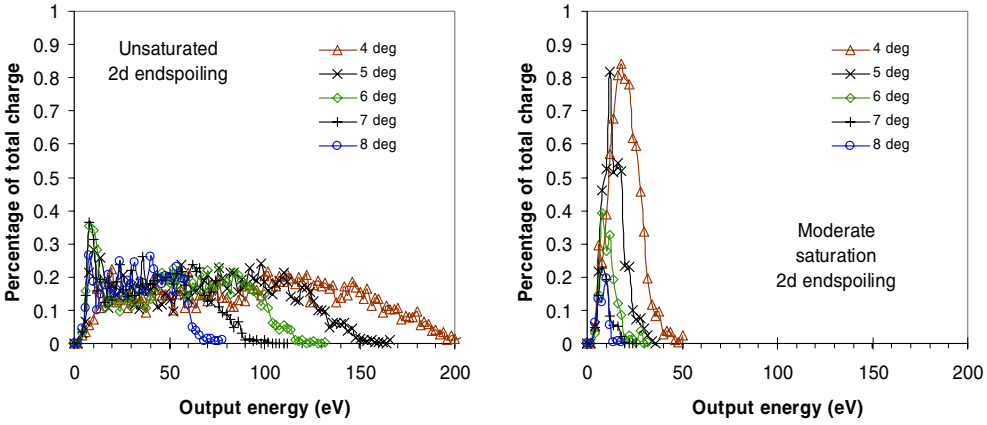

Fig. 6. Differential output energy distributions calculated at given output angles (shown in the legend). The average output energy and energy spread are substantially reduced at saturation.

Another possible way to optimize the source brightness is to modify the channel end-spoiling (the electrode penetration into the pore). The output distributions calculated for the MCA pores with different penetration are shown in Fig. 7. These results indicate that some end-spoiling has to be present at the pore output in order to achieve the best source performance. In addition to electrode penetration it is possible to consider different geometries of the output electrode, some of which have already been shown to improve the brightness of electron sources by optimizing the extraction electric field [16].

The results of modeling will be correlated with the experimental data on the MCA output distributions to be measured in the near future.

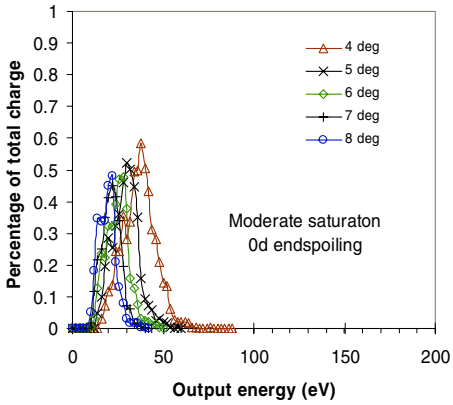

Fig. 7. The same as in Fig. 6 except with no electrode penetration into the channel (no end-spoiling). The average output energy and energy spread are smaller for MCA with electrode penetration (compare with Fig. 6.b).

Acknowledgments

This work was partially funded by DARPA grant HR0011-05-9-0001.

References

[1] A.S. Tremsin, D.R. Beaulieu, H.F. Lockwood, Microelectronic Engineering 83 (2006) 990.
[2] N. Koshida, M. Hosobuchi, Rev. Sci. Instr. 56 (1985) 1329.
[3] N. Koshida, Rev. Sci. Instr. 57 (1986) 354.
[4] I.M. Bronstein, A.V. Evdokimov, V.M. Stozharov, et al., Radiotekhnika i Elektronika 24 (1979) 871.
[5] G.J. Price, G.W. Fraser, Nucl. Instr. Meth. A 474 (2001) 188.
[6] P.M. Shikhaliev, Nucl. Instr. Meth. A 420 (1999) 202.
[7] L. Giudicotti, Nucl. Instr. Meth. A 480 (2002) 670.
[8] Munro's Electron Beam Software Ltd. http://www.mebs.co.uk/
[9] P. Wurz, L. Gubler, Rev. Sci. Instr. 67 (1996) 1790.
[10] A S. Tremsin, J.F. Pearson, J.E. Lees and G.W. Fraser, Proc. SPIE 2518 (1995) 384.
[11] E.A. Burke, IEEE Trans. Nucl. Sci. NS-24 (1977) 2505.
[12] A.J. Dekker, Solid State Physics: Secondary Electron Emission, Academic Press, New York, 1958.
[13] G.E. Hill, Adv. Electron. Electron Phys. A 40 (1976) 153.
[14] J. R. Young, J. Appl. Phys. 28 (1957) 524.
[15] I.R. Petrova, Yu.A. Flegontov, Sov. J. Opt. Tech. 55 (1988) 210.
[16] Q. Ji, X. Jiang, T.-J. King, K.-N. Leung, K. Standiford, and S.B. Wilde, J. Vac. Sci. Tech. B 20 (2002) 2717.